Geoscientific

Model Development

Discussions

The co-condensation of semi-volatile organics into multiple aerosol particle modes

Matthew Crooks[1], Paul Connolly[1], David Topping[1], and Gordon McFiggans[1]

[1]The School of Earth, Atmospheric and Environmental Science, The University of Manchester, Oxford Road, Manchester, M13 9PL

Correspondence to: matthew.crooks@manchester.ac.uk

Abstract. An existing equilibrium partitioning model for calculating the equilibrium gas/particle concentrations of multiple semi-volatile organics within a bulk aerosol is extended to allow for multiple core aerosol modes of different sizes and chemical compositions. In the bulk aerosol problem the partitioning coefficient determines the fraction of the total concentration of semi-volatile material that is in the condensed phase on the aerosol. This work modifies this definition for multiple polydisperse aerosol modes to account for multiple condensed concentrations; one for each semi-volatile on each core aerosol mode. The pivotal assumption in this work is that each aerosol mode contains a core constituent which is involatile thus overcoming the potential problem of smaller particles evaporating completely and then condensing on the larger particles to create a monodisperse aerosol at equilibrium. The resulting coupled non-linear system is approximated by a simpler set of equations in which the organic mole fraction in the partitioning coefficient is set to be the same across all modes. By perturbing the condensed masses about this approximate solution a correction term is derived which accounts for much of the removed complexities. This method offers a greatly increased efficiency in calculating the solution without significant loss in accuracy, thus allowing its inclusion into large scale models feasable.

1 Introduction

Volatile and semi-volatile compounds are of key importance to a wide variety of industries (Biniecka and Caroli (2011)) including atmospheric science (Topping et al. (2013), Topping and McFiggans (2012)), pharmaceuticals (Sitaramaraju et al. (2008), Wang et al. (2011)), food and drink (Vernocchi et al. (2008), de Roos (2003), Hui et al. (2010), Mendes et al. (2012)), water treatment (Zarra et al. (2009)) and perfume (Morris (1984)). Many of these industries exploit the aromatic properties of a large number of semi-volatiles and an understanding of their behaviour is crucial in order to identify, produce and capture certain aromas as well as controlling the rate of their subsequent evaporation in, for example, the perfume industry. In the water treatment sector the aromatic properties are not considered a favourable quality and inhibiting their release is important. The production of volatile compounds from all of these industries, however, can have far reaching negative consequences on

Geoscientific
Model Development
Discussions

both health and the environment (Klein (1995), Epstein and Gibson (2013), Wu et al. (2009)) as well as influencing weather and climate (Morgan et al. (2010), Morris (1984)).

This paper approaches the study of semi-volatile compounds from an atmospheric and cloud
30 physics perspective but the equilibrium partitioning theory presented herein is applicable to the wide variety of problems outlined above. The condensed phases of the semi-volatile compounds in the atmosphere occur within aerosol particles which can have a profound effect on cloud properties and climate. The ability of an aerosol particle to act as a cloud condensation nucleus (CCN) is determined by many factors including size, number concentration and chemical composition, as well as
35 the supersaturation of the air (Pruppacher and Klett (1977)). An increase in number concentration of a monodisperse aerosol which acts as a CCN will, in general, produce a greater number of smaller cloud droplets as there are more particles competing for the same available water (Twomey (1959)). In contrast, according to Köhler theory, the larger aerosol particles in a polydisperse system will have a greater affinity to activate into cloud droplets and their presence can deplete the available
40 water vapour more quickly, due to their quicker growth rates. Consequently, this can suppress the supersaturation which prevents the smaller particles from activating (Ghan et al. (1998)).

The aforementioned effects of aerosol size and number concentration can alter the precipitation rate and, as a result, the lifetime of clouds (Stevens and Feingold (2009), Albrecht (1989)). In addition to a direct effect of an increase in number of cloud droplets leading to both an increase in
45 reflected shortwave radiation and absorbed longwave radiation (McCormick and Ludwig (1967), Chýlek and Coakley Jr (1974)) there is a complicated interdependency between cloud longevity and albedo (Twomey (1974), Twomey (1977)). The result is an approximate -0.7 W m^{-2} increase in mean global radiative forcing; although this is subject to a large degree of uncertainty, which is on the order of the total radiative forcing from anthropogenic activity (Connolly et al. (2014), IPCC
50 (2013), Lohmann et al. (2000)).

Quantifying the size and chemical composition of individual aerosol particles within a population is complicated due to them being a heterogeneous mix of primary and secondary aerosol. Primary aerosol particles are mostly emitted directly from biogenic and anthropogenic sources. Although some models exist to simulate semi-volatile primary particles (Tsimpidi et al. (2014)) in this paper
55 they are assumed to be non-volatile so that they remain in the condensed phase. Secondary aerosol forms by condensation of gases onto the particles. This process is fairly well understood for inorganic gases (Hallquist et al. (2009)), however, there is significant uncertainty associated with the formation of secondary organic aerosol (SOA) from volatile organic compounds (VOCs). Part of this uncertainty is a result of the poorly quantified process of oxidation of VOCs to produce SOA
60 and other VOCs with reduced volatility (Jimenez and et. al. (2009), Yu (2011)).

Over remote continental regions between 5% and 90% of the total aerosol mass can be made up of organic material (Andreae and Crutzen (1997), Zhang et. al. (2007), Gray et al. (1986)) and a significant proportion of this can be from secondary sources. SOA in such large quantities will act to

increase the size of the particles as well as significantly changing their chemical composition. The
effect of the increased size, and consequently soluble mass, is found to be the dominant effect on
cloud; increasing the number of cloud droplets and subsequently decreasing the critical supersatura-
tion (Dusek et al. (2006), Topping et al. (2013)).

It is estimated that $10^4 - 10^5$ organic species have been measured in the atmosphere but this may
only be a small proportion of the total (Goldstein and Galbally (2007)). Of this number fewer than
3000 have actually been identified (Hildemann et al. (1991)). It is, therefore, impractical to try to
model each compound individually and two popular methods have been developed to simulate mul-
tiple organic species using equilibrium absorptive partitioning theory (Pankow (1994)); a method
of calculating the equilibrium condensed concentrations without solving the computationally ex-
pensive dynamic condensation and evaporation processes. The first noteworthy approach (Odum
et al. (1996)) proposes an empirically fitted relation derived from two-compound experiments which
benefits from its simplicity but, as with any empirical relation, has possibly limited applicability
outside of the original constraints. In particular, these models are found to be unrealistically sensi-
tive to changes in concentration of the organics (Cappa and Jimenez (2010)). The second (Donahue
et al. (2006)) uses a volatility basis set; binning large numbers of semi-volatile organic compounds
(SVOCs) into a small number of representative species with effective saturation concentrations. This
method was later extended to account for the co-condensation of both water and SVOCs (Barley
et al. (2009)) by treating the water as an additional volatile substance. All models for finding the
equilibrium vapour/condensed phases of multiple SVOCs are currently restricted to a single aerosol
mode.

In this paper we present a model for the co-condensation of water and SVOCs onto multiple core
aerosol modes using the volatility basis set method of Donahue et al. (2006). By considering the
core aerosol to be involatile we remove the possibility that the smaller particles evaporate completely
thus allowing the larger particles to take up additional condensed mass to produce a monodisperse
aerosol at equilibrium. The concentration of a SVOC in the condensed phase on one mode has the
effect of reducing the total concentration available to the other modes and as a result the equilibrium
vapour/condensed phases of all the organics on all the core modes must be solved for simultaneously.
By assuming all modes have approximately the same organic mole fraction a method of solution is
derived which has a high degree of accuracy while being significantly more efficient than a stan-
dard numerical algorithm would be. Condensed concentrations of organics are compared against
equilibrium calculated from a modified parcel model and are found be comparable.

2   Equilibrium Absorptive Partitioning Theory for Size Independent Bulk Aerosol

Before introducing the new multiple mode equilibrium partitioning theory, we first review existing
partitioning theories, beginning with that for a bulk aerosol, (Donahue et al. (2006)). Multiple organic

species are binned according to their saturation concentration, C_j^*, using a $\log_{10}$ volatility basis set
with values from $1 \times 10^{-6} \mu$ mol m^{-3} to $1 \times 10^3 \mu$ mol m^{-3} (Cappa and Jimenez (2010), Donahue
et al. (2006)). The value of C_j^* is proportional to the saturation vapour pressure, p_j^o (atm), of the
organics in the jth bin through

$$C_j^* = \frac{p_j^o \gamma_j 10^6}{RT}. \tag{1}$$

Here γ_j is the activity coefficient of the organics in the jth bin, R is the universal gas constant (m^3
atm mol^{-1}K^{-1}), and T is the temperature (K) which is taken to be 298.15K.

Water and other inorganic semi-volatile compounds can additionally be considered by binning
them along with the organics. For simplicity we ignore inorganic semi-volatiles and for the purposes
of applying the theory to the particular problem of cloud physics later in the paper we treat water as
a seperate volatile compound so that its abundance can be varied independently of the organics.

The total concentration of the semi-volatile in the jth volatility bin is defined by C_j (μ mol m^{-3})
and is decomposed into a vapour and a condensed phase,

$$C_j = C_j^v + C_j^c, \tag{2}$$

indicated by the superposed v and c respectively. The total concentration of all compounds in the
condensed phase, C_{OA}, is the sum of the concentration of ions of core aerosol, C^o, the condensed
water, C^w, and each organic component in the condensed phase,

$$C_{OA} = C^o + C^w + \sum_k C_k^c. \tag{3}$$

The condensed water can be calculated assuming ideality by equating the relative humidity, R_H, to
the mole fraction of water,

$$R_H = \frac{C^w}{C^o + C^w + \sum_k C_k^c}. \tag{4}$$

Equation (4) can be rearranged to make C^w the subject and then substituted into (3) and factorised
to give

$$C_{OA} = \frac{1}{1 - R_H} \left(C^o + \sum_k C_k^c \right). \tag{5}$$

The analogous expression to (4) for the organics is

$$\frac{C_j^v}{C_j^*} = \frac{C_j^c}{C_{OA}}, \tag{6}$$

where the relative humidity has been replaced by the ratio of the vapour pressure to the saturation
vapour pressure of the jth component using (1).

Eliminating C_j^v from (2) using (6) and rearranging gives the condensed concentration of the jth
organic component in terms of the total concentration

$$C_j^c = C_j \left(1 + \frac{C_j^*}{C_{OA}} \right)^{-1}. \tag{7}$$

Geoscientific
Model Development
Discussions

130   The partitioning coefficient is defined as

$$\xi_j = \left(1 + \frac{C_j^*}{C_{OA}}\right)^{-1},$$ (8)

so that $C_j^c = \xi_j C_j$. Since C_{OA} depends on the C_j^c this problem must be solved iteratively.

3   Equilibrium Absorptive Partitioning Theory for a Monodisperse Aerosol

The theory in the previous section is independent of the size of the aerosol particles. We extend this

135   theory to include size dependence for a monodisperse aerosol. The partitioning of water is influenced

by the size of the aerosol through the Kelvin factor,

$$K^w = \exp\left(\frac{4M_w \sigma}{\rho_w RTd}\right),$$

where M_w, ρ_w and σ are the molecular weight, density and surface tension of water, and d is the

diameter of the wet aerosol particles. The Kelvin factor multiplies the right-hand side of equation

140   (4), see, for example, Rogers and Yau (1996),

$$R_H = \frac{C^w K^w}{C^o + C^w + \sum_k C_k^c}.$$ (9)

Consequently, the right hand side of equation (5) becomes

$$C_{OA} = \frac{K^w}{K^w - R_H}\left(C^o + \sum_k C_k^c\right),$$ (10)

and for notational simplicity we define the prefactor on the right-hand side by η,

145   $$\eta = \frac{K^w}{K^w - R_H}.$$

The Kelvin factor for the organics, K_j, is defined by Cai (2005) as

$$K_j = \exp\left(\frac{4M_j \sigma}{\rho_j RTd}\right),$$ (11)

where M_j and ρ_j are the molecular weight and density of the organics in the jth volatility bin, and

σ is the surface tension of the particle with condensed organics and water. This is included into

150   equation (6) in an analogous way to the Kelvin factor for water to give

$$\frac{C_j^v}{C_j^*} = \frac{C_j^c K_j}{C_{OA}},$$ (12)

and consequently the partitioning coefficient is defined as

$$\xi_j = \left(1 + \frac{C_j^* K_j}{C_{OA}}\right)^{-1}.$$ (13)

4 Equilibrium Absorptive Partitioning Theory for a Conglomoration of Particles of Multiple Sizes and Composition

An aerosol population commonly comprises particles of different sizes and chemical composition. In this section we consider aerosol which can be decomposed into multiple monodisperse aerosol modes. We propose a novel extension to the theory of the previous sections which is applicable to these more diverse conglomerations of particles and therefore suitable for application to a wider class of problems.

The most significant change to the theory for multple modes is that the equations must explicitly take into account that a single molecule of an organic cannot condense onto more than one core mode. Consider the 10 organic molecules and 2 core particles shown in blue and green respectively in Figure 1. Suppose the subset highlighted in pink are known to condense onto the left core particle; these molecules cannot also condense onto the right particle. Hence, the only the molecules available to condense onto the right core particle are those circled by the dashed line. The converse is also true; if the molecules highlighted in pink in Figure 2 are known to condense onto the right particle then only the remaining molecules are free to condense onto the left particle. As such, the concentration of organics in the jth volatility bin which is available to the ith mode is the total concentration in the jth volatility bin minus the condensed concentrations of the organics in the jth bin on the other modes. It is this quantity that is multiplied by the partitioning coefficient in the multiple mode case.
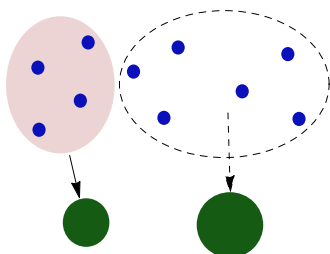
Figure 1. A representation of the condensation of a SVOC, shown by the blue dots, onto two non-volatile particles, shown by the green circles. The SVOC is divided into two groups; those that condense onto the left core particle and those remaining to equilibriate on the right particle.

We make the following changes to extend the theory in the previous section to the multiple mode case:

- The condensed mass of the jth organic component will now be split across several core modes. Define the condensed concentration of the jth organic species on the ith core mode by C_{ij}^c so

Geoscientific
Model Development
Discussions
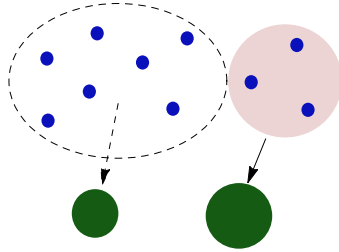
Figure 2. Same as Figure 1 but with the two non-volatile particles swapped.

that the condensed phase C_j^c can we expressed as the sum

$$C_j^c = \sum_r C_{rj}^c. \tag{14}$$

For consistency, a subscript i refers to the core mode and j refers to the jth volatility bin. Dummy indices r and k are used in the summations to make clear which terms are being summed and are restricted to sums over i and j, respectively. Subsequently, the total concentration of semi-volatiles in the jth volatility bin is decomposed into a single vapour phase and the sum of the multiple condensed phases

$$C_j = C_j^v + \sum_r C_{rj}^c. \tag{15}$$

The total concentration in the condensed phase on the ith mode is given by the sum of the concentrations of the core and all of the condensed organics and water on the ith mode,

$$C_{OA,i} = C_i^o + C_i^w + \sum_k C_{ik}^c,$$

which can equally be expressed in an analogous way to (10) as

$$C_{OA,i} = \frac{K_i^w}{K_i^w - R_H} \left(C_i^o + \sum_k C_{ik}^c \right). \tag{16}$$

Here

$$K_i^w = \exp\left(\frac{4 M_w \sigma}{\rho_w R T d_i} \right),$$

is the Kelvin factor of water and C_i^o is the number of μ mol per cubic meter of the ith core aerosol mode. d_i is the diameter of the ith mode with both condensed water and organics. For notational simplicity we define

$$\eta_i = \frac{K_i^w}{K_i^w - R_H}, \tag{17}$$

195   so that (16) can be written as

$$C_{OA,i} = \eta_i \left(C_i^o + \sum_k C_{ik}^c \right). \tag{18}$$

– The partitioning coefficient, given by (13), depends on the material properties and size of the core aerosol, through C_{OA} and K_j, and consequently each volatility bin can have a different coefficient for each core mode. The Kelvin factor for the jth volatility bin, (11), is modified

200   to depend on the diameter of the ith composite mode, d_i,

$$K_{ij} = \exp \left(\frac{4 M_j \sigma}{\rho_j R T d_i} \right),$$

Subsequently, the multiple mode analogy to (12) on the ith core mode is

$$\frac{C_j^v}{C_j^*} = \frac{C_{ij}^c K_{ij}}{C_{OA,i}}, \tag{19}$$

This can be used to eliminate the vapour concentration from (15)

205    $$C_j = \frac{C_j^* C_{ij}^c K_{ij}}{C_{OA,i}} + \sum_r C_{rj}^c. \tag{}$$

The concentration C_{ij}^c can be extracted from the sum on the right-hand side and the equation rearranged to give

$$C_j - \sum_{r \neq i} C_{rj}^c = C_{ij}^c \left(1 + \frac{C_j^* K_{ij}}{C_{OA,i}} \right). \tag{20}$$

We denote the partitioning coefficient for the jth organic component onto the ith core mode

210   by ξ_{ij} and define it in an analogous way to (13),

$$\xi_{ij} = \left(1 + \frac{C_j^* K_{ij}}{C_{OA,i}} \right)^{-1}. \tag{21}$$

– The total concentration of the jth organic which is available to the ith core mode, as previously discussed, can now be defined

$$C_{ij} = C_j - \sum_{r \neq i} C_{rj}^c,$$

215   or alternatively

$$C_{ij} = C_j - \sum_r C_{rj}^c + C_{ij}^c. \tag{22}$$

– An expression for the condensed concentration of the jth organic on the ith core mode can now be expressed as the product of the partitioning coefficient with C_{ij},

$$C_{ij}^c \;=\; \frac{C_j - \sum\limits_r C_{rj}^c + C_{ij}^c}{1 + \dfrac{C_j^* K_{ij}}{C_{OA,i}}}, \tag{23}$$

which is a rearrangement of (20). Replacing $C_{OA,i}$ using (18) yields

$$C_{ij}^c \;=\; \frac{C_j - \sum\limits_r C_{rj}^c + C_{ij}^c}{1 + \dfrac{C_j^* K_{ij}/\eta_i}{C_i^o + \sum\limits_k C_{ik}^c}}. \tag{24}$$

The non-linear nature of these equations poses a problem for obtaining a solution. Numerical methods exist for solving such problems but require an initial guess for the solution. Furthermore, there are multiple unknowns and multi-dimensional non-linear solvers are too computationally expensive to implement in a global climate model. In the remainder of the paper we present a method for obtaining an approximate solution to equations (24) which facilitates a numerical solver in computing the full solution. This approximation, however, is sufficiently accurate that an analytic perturbation method, derived in Section 6, can be used to reduce the inaccuracies and render the costly numerical solution redundant.

5 Quasi-leading order solution

5.1 Motivation

Low accuracy solutions to equations (24) for the equilibrium concentration in the condensed phase can be found using a brute force trial and error method. 30 such solutions for between 2 and 5 core modes are shown in Figure 3 with each calculated using different randomised inputs for the parameters taken from Table 1. The concentrations of organics in each volatility bin are kept in the proportions shown in Table 2 but are rescaled by a random factor of between 0 and 100. Plotted in the graph is the total organic mole fraction which we define as the concentration of semi-volatile material on a mode divided by the total number of ions in the aerosol. For the ith mode this is

$$\theta_i = \frac{\sum\limits_k C_{ik}^c}{C_i^o + \sum\limits_k C_{ik}^c}, \tag{25}$$

Each solution is represented by several dots joined by a vertical line with the y coordinate of the dots showing the mole fraction of one of the modes. These are plotted against the average mole fraction

Geoscientific
Model Development
Discussions

of all the modes in that solution on the x axis. As can be seen from Figure 3, even though the mole fractions are different, they never deviate too far from the mean, shown by the dashed line. Assuming the same mole fraction for all the modes allows approximate values of $C_{OA,i}$ to be found in terms of a single parameter. This greatly simplifies the problem and can provide a reasonable guess for the non-linear solver.

We emphasise that although the mole fractions of the different modes are comparable, the equilibrium partitioning solution is still dependent on the individual material properties of the core aerosol with number concentration, size, molecular weight, density and van't Hoff factors all influencing the number of moles in the core and consequently the number of moles of condensed organics required to give the appropriate mole fraction.
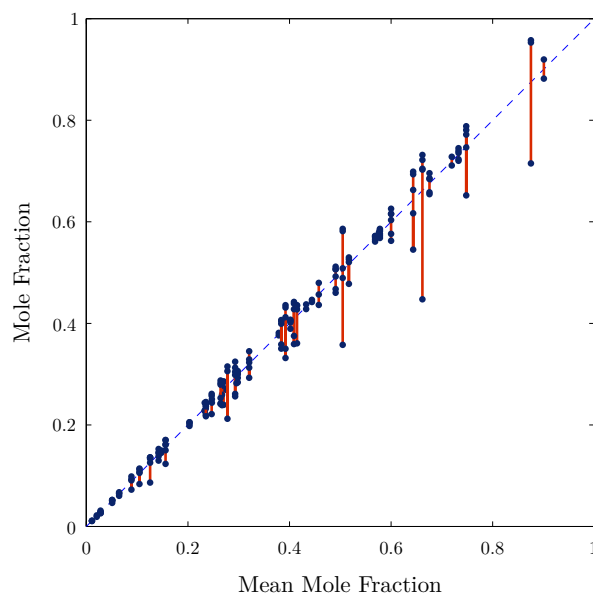
Figure 3. The mole fractions of multiple different core aerosol modes plotted against mean mole fraction on the x axis. 30 solutions are shown with parameters randomly chosen from the ranges shown in Table 1 with $R_H = 0\%$.

Table 1. Randomised variables used to plot Figure 3. n_i, D_i, ρ_i^o and M_i^o are the number concentration, diameter, density and molecular weight of the ith core aerosol, respectively. ν_i^o and ν_j are the van't Hoff factors of the core and organics.

variable	n_i (pcc)	D_i (nm)	ρ_i^o (kg m^{-3})	ρ_i (kg m^{-3})	M_j, M_i^o (kg mol^{-1})	ν_i^o	ν_j
min	50	50	500	500	0.1	1	0
max	500	500	2000	1500	0.4	3	1

Geoscientific
Model Development
Discussions

Table 2. The distribution of total concentrations of organics used in the simulations.

$\log_{10} C^*$	-6	-5	-4	-3	-2	-1	0	1	2	3
$C_j(\mu \text{ mol m}^{-3})$	0.005	0.01	0.02	0.03	0.06	0.08	0.16	0.3	0.42	0.8

5.2 Derivation of a Solution with an Average Mass Fraction

The solution derived under the assumption of a common mole fraction, θ, is referred to as the quasi-leading order solution and is denoted, $\bar{C}_{ij}^c$. Rearranging (25) with θ_i replaced by θ gives

$$\frac{\theta}{1-\theta} = \frac{\sum_k \bar{C}_{ik}^c}{C_i^o}.$$

The left-hand side of this equation is the same for all the modes and consequently the right-hand side must also be the same. For notational simplicity we combine the left-hand side into a single parameter, β,

$$\beta = \frac{\theta}{1-\theta} = \frac{\sum_k \bar{C}_{ik}^c}{C_i^o}, \tag{26}$$

and subsequently

$$\sum_k \bar{C}_{ik}^c = \beta C_i^o. \tag{27}$$

The wet diameter of the combined aerosol is assumed to be sufficiently large that the Kelvin factors for the SVOC can be approximated by 1. The same is not true for the Kelvin factors for water, K_i^w. If these are assumed to take the value 1 then the definition of η_i, as given by (17), will lead to a gross over estimate of the condensed water close to cloud base, becoming infinite as the relative humidy becomes 1.

The governing equations for quasi-leading order solution are obtained by making the approximation given by (27) together with setting $K_{ij} = 1$,

$$\bar{C}_{ij}^c = \frac{C_j - \sum_r \bar{C}_{rj}^c + \bar{C}_{ij}^c}{1 + \dfrac{C_j^*/\eta_i}{C_i^o(1+\beta)}}. \tag{28}$$

The interdependence of the $\bar{C}_{ij}^c$ can be eliminated to obtain an explicit expression for each in terms of the mole fraction β,

$$\bar{C}_{ij}^c = \frac{C_i^o(1+\beta)(1-\phi_j(\beta,\eta_i))C_j}{C_j^*/\eta_i}, \tag{29}$$

the algebra of this step is given in A. The dependence of ϕ_j, given by (A2), is expressed explicitly for clarity. Both sets of equations are equivalent to one another and either can be used to find the

11

Geoscientific

Model Development

Discussions

EGU

Open Access

275 $\bar{C}_{ij}^c$. The coupled nature of equations (28), however, requires a matrix inversion to solve and this will take more time to calculate than the solution to equations (29).

The complexity of the summation of $\bar{C}_{ij}^c$ in the denominator has now been removed in favour of a single parameter, β. This can be solved for using a much quicker one-dimensional root find algorithm which iterates the value of β and solves the linear system of equations at each step to

280 find $\bar{C}_{ij}^c$. Equations (28) together with solving equation (26) for each value of i produces an over determined system for $\bar{C}_{ij}^c$ and β with more equations than unknowns. To overcome this we only solve (26) for $i = 1$.

While the dependence of η_i on $\bar{C}_{ij}^c$ has not been removed it is sufficiently weak that the values of $\bar{C}_{ij}^c$ calculated at the previous iteration of β can be used to evaluate the Kelvin factor for water and

285 therefore η_i; simultaneously converging on the correct value as β is found.

5.3 Results

The quasi-leading order solution given in the previous section is calculated and used as an initial guess for solver of the full non-linear problem; a comparison of the two solutions are presented here. In order to test the theory over a large parameter space values of the inputs are chosen from Table

290 1 and the models are run for between 2 and 6 modes. Solutions from only one mode are plotted for each run to avoid a bias towards the solutions for 6 mode runs which would otherwise have three times as many points plotted as the 2 mode runs.

Figure 4 shows the individual condensed masses of the 10 volatility bins, each with different shaped points. The blue dashed line shows equality between the approximation and the full solution

295 and the green dashed lines show 50% inaccuracies in the approximations. The very strong correlation between the full non-linear solution and the quasi-leading order solution demonstrates that the assumption of a common mole fraction made in the previous section not only offers an efficient way of calculating an initial guess for the non-linear solver but actually offers an accurate approximation to the solution for the condensed masses of the organics.

300 Figure 5 compares the organic mass fractions, defined as the total mass of condensed organics divided by the total mass of the aerosol, from the full non-linear solution and the quasi-leading order solution from the different runs. A range of relative humidities and van't Hoff factors of the core aerosol are used; these values are shown above each plot. Small values of the van't Hoff factor appear to have a significant effect on the mass fraction as the correlation of the right-hand three plots

305 is worse. This is caused by the need to divide by the van't Hoff factor when converting from number of ions to mass. The result is a high sensitivity of the mass to slight inaccuracies in the number of ions for van't Hoff factors close to zero; this is addressed in Section 6.

Similarly, lower values of the relative humidy reduce the correlation of the two solutions with almost perfect agreement in the lower two plots for $R_H = 99.999\%$. This is likely a result of higher

310 relative humidities increasing the wet diameter of the droplets and subsequently reducing the Kelvin

Geoscientific

Model Development

Discussions
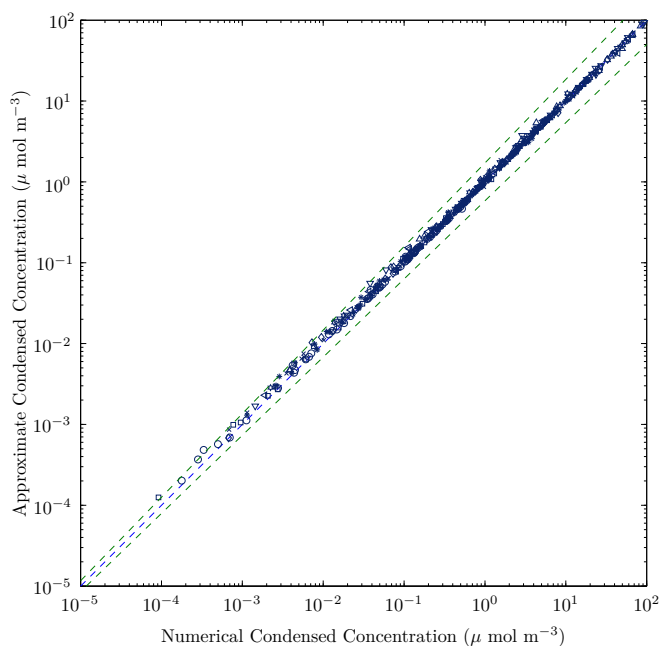
Figure 4. Comparison of the condensed concentrations of organics from the quasi-leading order solution against that calculated using the non-linear solver for randomly chosen parameters from Table 1. The solution is calculated for between 2 and 6 modes and only the condensed concentrations on the first mode are plotted. The different volatility bins are distinguished by the shape of the points. Equality between the solutions is shown by the dashed blue line and the green lines shown where the approximation over or under estimates by a factor of 2.

factor closer to 1. Since the quasi-leading order solution sets the Kelvin factors of the organics to 1, higher values of R_H improve this approximation. At $R_H = 99.999\%$ there increased water contend of the wet aerosol will further act to increase the value of C_{OA} and subsequently lead to a significantly higher proportion of the organics being in the condensed phase. With nearly all the organics in the condensed phase there is much less potential for errors in the approximation.

6 Perturbation Solution

Although the condensed masses computed using the approximation derived in Section 5 did not completely agree with the full non-linear solution, the errors were small relative to the size of the C_{ij}. We propose a correction term to this approximation which improves the accuracy and also takes into account the Kelvin terms. Suppose the actual condensed masses, C_{ij}^c, can be obtained from the
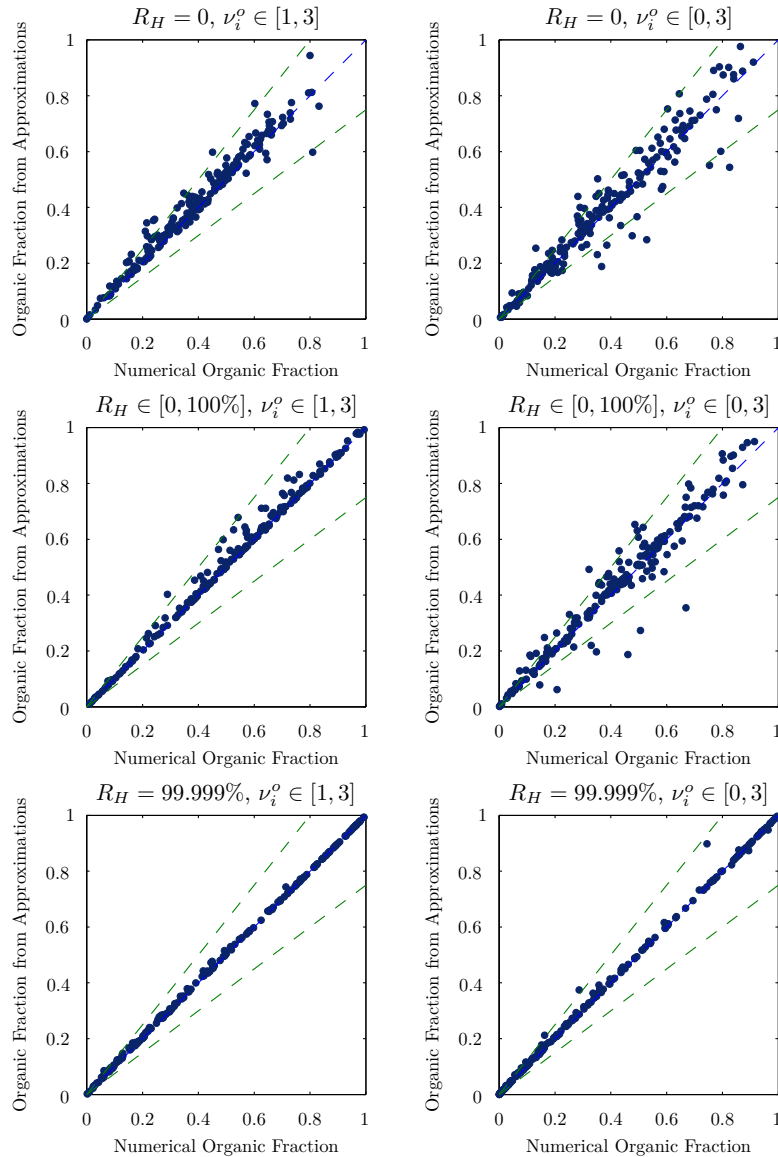
Figure 5. Comparison of the organic mass fraction from the two approximations against that calculated using the non-linear solver for randomly chosen parameters from Table 1. The solution is calculated for between 2 and 6 modes and only the mass fraction of the first is plotted. 25% error margins are shown by the dashed green lines.

quasi-leading order solution, $\bar{C}_{ij}^c$, by adding a small perturbation

$$C_{ij}^c = \bar{C}_{ij}^c + \hat{C}_{ij}^c,$$

Geoscientific

Model Development

Discussions

where we assume $|\hat{C}_{ij}^c| \ll |\bar{C}_{ij}^c|$. The Kelvin factors also depend on the final condensed mass and for clarity ought to be written $K_{ij} = K_{ij}(C_{ij}^c)$. This, however, adds much complexity. Therefore, it is assumed that the quasi-leading order solution provides a suitably accurate approximation to the condensed masses of semi-volatiles for the purposes of calculating the Kelvin factors. Consequently, we make the additional approximation $K_{ij}(C_{ij}^c) \approx K_{ij}(\bar{C}_{ij}^c)$ which we denote $\bar{K}_{ij}$. Similarly, $K^w(C_{ij}^c) \approx K^w(\bar{C}_{ij}^c)$ and consequently $\eta_i(C_{ij}^c) \approx \eta_i(\bar{C}_{ij}^c) = \bar{\eta}_i$. We substitute the perturbation into the equations (24) together with these approxations to give

$$\bar{C}_{ij}^c + \hat{C}_{ij}^c = \frac{C_j - \sum\limits_r \bar{C}_{rj}^c + \bar{C}_{ij}^c - \sum\limits_r \hat{C}_{rj}^c + \hat{C}_{ij}^c}{1 + \dfrac{C_j^* \bar{K}_{ij}/\bar{\eta}_i}{C_i^o + \sum\limits_k \bar{C}_{ik}^c + \sum\limits_k \hat{C}_{ik}^c}}. \tag{30}$$

Assuming the perturbed quantities, $\hat{C}_{ij}^c$, are small we can linearise these equations to give

$$\left(1 - \bar{\xi}_{ij}\right)\hat{C}_{ij}^c + \bar{\xi}_{ij}\sum\limits_r \hat{C}_{rk}^c - \mathcal{L}_{ij}\sum\limits_k \hat{C}_{ik}^c = \frac{C_j - \sum\limits_r \bar{C}_{rj}^c + \bar{C}_{ij}^c}{1 + \dfrac{C_j^* \bar{K}_{ij}/\bar{\eta}_i}{C_i^o + \sum\limits_k \bar{C}_{ik}^c}} - \bar{C}_{ij}^c. \tag{31}$$

the algebra for which is given in B. The $\bar{\xi}_{ij}$ are the partitioning coefficients, (21), calculated using the quasi-leading order solution; explicit expressions are given by (B2). The $\mathcal{L}_{ij}$ are defined in B and are coefficients that depend on the $\bar{C}_{ij}^c$ as well as the parameters of the problem but are independent of the perturbations. Therefore, these equations are linear in the perturbations and can be solved much quicker than the full set of non-linear equations.

If the quasi-leading order solution, $\bar{C}_{ij}^c$, were the exact answer then the right-hand side would be simple a rearrangement of the equations (24) and would be zero. In such a situation, the left-hand side would also have to be zero resulting in a homogeneous system of coupled linear equations with only the trivial solution in which $\hat{C}_{ij}^c = 0$. However, the quasi-leading order solution does not satisfy the full system of equations but is "close" by some measure. Consequently, the right-hand side of (31) is "small" and defines the size of the small perturbation $\hat{C}_{ij}^c$. The additional correction term can be calculated by a simple matrix inversion owing to the linear nature of equations (31) which, as we shall see in the following section, produces a much more accurate solution in a fraction of the time it would take to run the non-linear solver.

6.1 Results

Figure 6 is a replica of Figure 4 with the addition of the condensed concentrations calculated using the first order correction term shown in red. The perturbation solution can be seen to offer an improved approximation to the quasi-leading order solution, especially above $0.1\,\mu\,\mathrm{mol}\,\mathrm{m}^{-3}$ where

Geoscientific

Model Development

Discussions
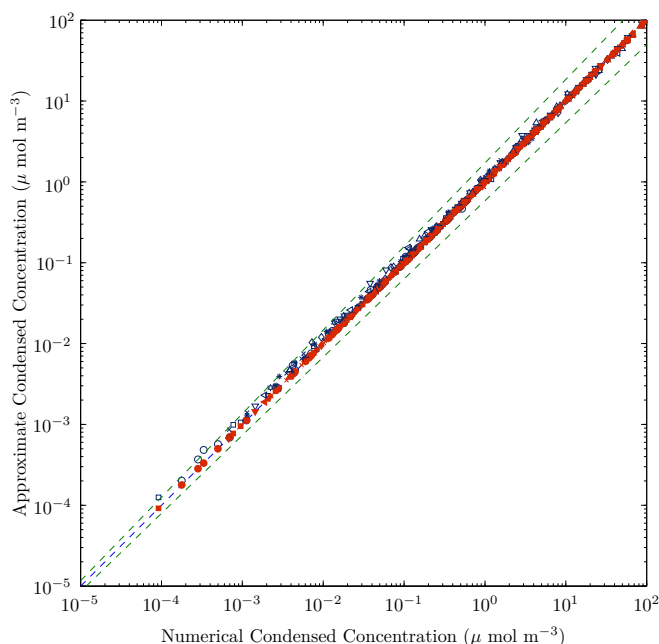
Figure 6. Same as Figure 4 with the addition of the perturbation solution shown in red.

the agreement with the non-linear solution is almost perfect. At lower concentrations the correction term reduces the degree to which the quasi-leading order approximation over predicts the condensed concentrations compared to the non-linear solution.

355   The organic mass fractions calculated from the perturbation solution are plotted against those calculated using the non-linear solver in Figure 7 and are shown in red. The graphs show a marked improvement on the quasi-leading order solution, which are shown in navy, across all parameter space. Adding the first order correction term reduces the errors to less than 20% in the worst cases of the top right plot compared to nearly 50% in the quasi-leading order solution. The general trends of

360   worse correlation for low R_H and ν_i^o observed in Figure 5 are replicated in the perturbation solution but to a much lesser extent. This is due to the inclusion of a leading order Kelvin factor for the organics that reduces the influence of the R_H and improvements in the accuracy of the condensed concentrations reduce the subsequent errors in the masses.

Figure 8 shows the percentage errors in the calculated mass fractions when compared to the solu-

365   tion from the non-linear solver. The top two plots, which had the worst correlation in Figure 7, show that the quasi-leading order solution produces errors in the organic mass fraction of below 20% in nearly all cases and these reduce to 10% when the correction term in the perturbation solution is included. The affect of van't Hoff factors close to zero is most notable in the middle two plots where the errors increase about 3 fold compared to when the van't Hoff factors are greater than 1; middle

370 right and left plots, respectively. The errors in the perturbation solution rarely exceed 10% across the
entire parameter space and are only a few percent at cloud base, shown by the lower 2 plots.
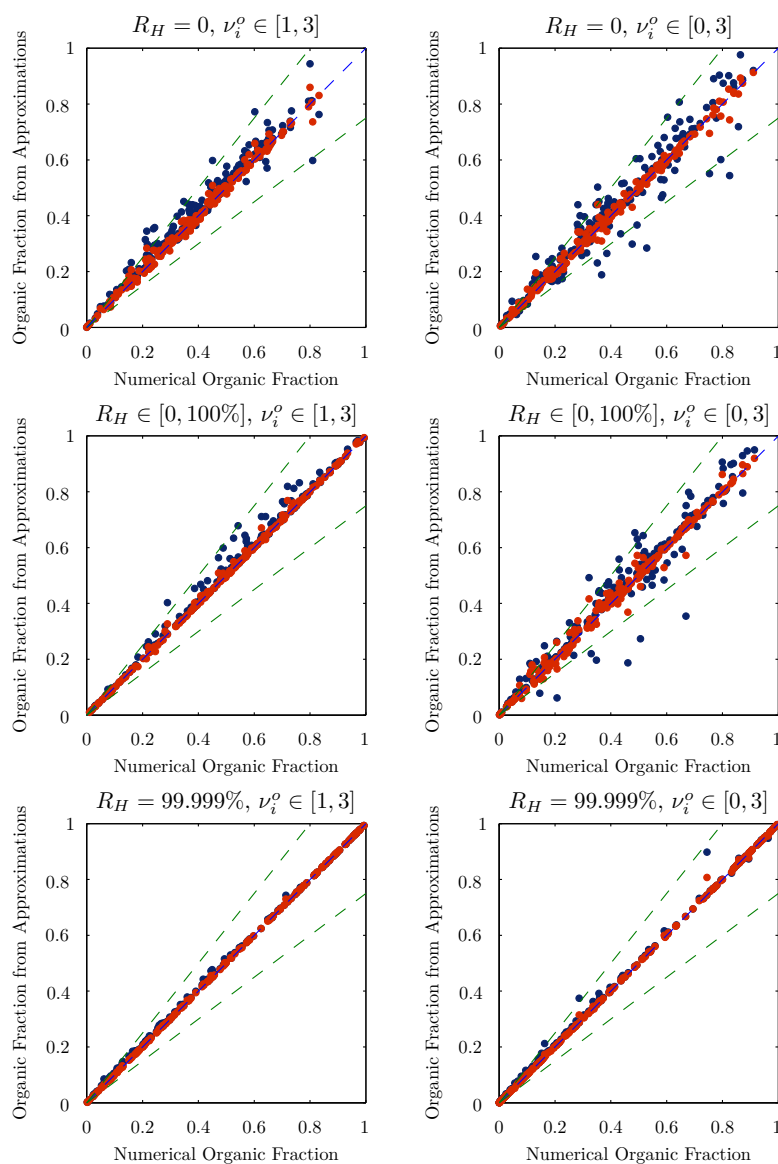
Figure 7. Same as Figure 5 with the addition of the perturbation solution shown in red.

Geoscientific
Model Development
Discussions

7 Comparison Between the Partitioning Theory and Parcel Model Simulations

The partitioning theory presented in the preceding sections calculates the equilibrium of each organic between the vapour and the condensed phases. If a dynamic model of condensation of organics is left to run for long enough it ought to equilibrate on the same solution. We test this here for two modes as verification of the extension of the partitioning theory to multiple modes.

A dynamic parcel model by Topping et al. (2013) is modified to maintain constant temperature, pressure and water vapour mass; the former two set to 293.15 K and 95000 Pa respectively and the latter is calculated from the specified relative humidity. In the simulations the time taken for small particles to grow to equilibrium is on the order of hundreds of seconds whereas larger particles take thousands. The large particles, however, should take up more of the condensed concentration of the organics due to their higher value of C_{OA}. As a consequence, the vapour phase equilibrates with the total condensed concentration very quickly but places too large a proportion on the smaller mode and insufficient on the larger. Due to the bulk system reaching equilibrium the large particles can only grow at the same rate that the small particles shrink and this process can take millions of seconds of simulation time to correct. We derive a more accurate initial condition by allowing time for the large particles to equilibrate with the vapour before placing the small particles into the model. This reduces the amount of organic vapour available to condense onto the smaller mode and prevents the gross over calculation of the condensed concentration on this mode in the initial time period.

Table 3. Material parameters used in the parcel model simulations.

variable	ρ_i^o (kg m^{-3})	ρ_j (kg m^{-3})	M_j (kg mol^{-1})	M_i^o (kg mol^{-1})	ν_i^o	ν_j
value	1770	1500	0.132	0.2	3	1

Table 4. Range of values assigned to the number concentration, n_i, and core diameter, D_i, used in the parcel model simulations.

variable	n_i (pcc)	D_i (nm)
mode 1	100-1000	25-100
mode 2	50	125

The parcel model was run twice with the parameters given in Tables 3 and 4. The first mode had a number concentration of 1000 pcc and a diameter of 50 nm in the first simulation and 100 nm in the second. The second mode was given initial periods of 300 and 10 seconds of simulation time, respectively, before the smaller mode was added. Subsequent time evolution of the condensed concentrations are shown by the solid lines in Figure 9 for a relative humidity of 50%. Bulk equilibrium is reached by about 1000 seconds with the individual modes reaching equilibrium by approximately

Geoscientific
Model Development
Discussions

20000 seconds. The parcel model converges on a value which is in excellent agreement with the partitioning theory shown by the dashed lines.

Figure 10 compares the condensed concentrations for a broader range of values of the diameter of the first mode; values are denoted above each plot. The top of the red sections of each bar depict the total condensed concentration in each volatility bin from the parcel model and the equivalent quantity from the partitioning theory is shown by the black crosses; the two agree almost exactly. The height of the green bar shows the condensed concentrations on the first mode from the parcel model and, as expected, an increase in diameter of these particles results in both an increase in total condensed concentration and the proportion of the which is on the first mode. The small particles of diameter 25 nm in the top left plot only account for a small proportion of the condensed concentration, as shown by the small area of green compared to the large area of red. When the size of these particles is increased to 100 nm they take up almost all of the organic material in the condensed phase; the lower right bars have a much larger area of green than red. The analogous quantities from the partitioning theory are shown by the dashed yellow lines which coincide with the tops of the green bars to a high degree of accuracy. The condensed concentrations on the second mode are shown by the height of the red sections of the bars which, when measured from the x axis, are shown by the horizontal black dashed lines across each bar. These too agree exceptionally well with the pink dashed lines which are the equivalent values from the partitioning theory.

Similar plots are shown in Figure 11 but this time the size of the first mode is fixed at 50 nm and the number concentration is varied instead; the values used are shown above each plot. As previously seen, the equilibrium partitioning theory agrees incredibly well with the parcel model simulations across the parameter space explored. Interestingly in these plots the total condensed concentration does not increase significantly when the number concentration of the first mode is increased from 100 pcc to 750 pcc. The proportion on each of the two modes, however, does increase, with almost equal amounts placed on each of the two modes when the first mode has a number concentration of 750 pcc.

7.1 Application to an Atmospherically Relevant Problem

Aerosol in the atmosphere is often characterised by multiple polydisperse modes with particles in each mode composed of a single chemical composition. The sizes of particles in each mode are described by size distributions which are a convenient way of treating a polydisperse aerosol as each size distribution can be considered as a single entity.

A common assumption is that the diameters of the particles, D, are lognormally distributed so that the number of aerosol particles, n, per logarithmic size interval is given by

$$\frac{dn}{d\ln D} = \frac{n_i}{\sqrt{2\pi}\ln\sigma} \exp\left[-\left(\frac{\ln\left(\frac{D}{D_m}\right)}{\sqrt{2}\ln\sigma}\right)^2\right].$$

Geoscientific
Model Development

Discussions

430 Here N is the total number of particles and D_m and σ are the median diameter and geometric standard deviation. Multiple lognormal size distributions can be added together to form more diverse aerosols

$$\frac{dn}{d\ln D} = \sum_i \frac{n_i}{\sqrt{2\pi}\ln\sigma_i} \exp\left[-\left(\frac{\ln\left(\frac{D}{D_{m,i}}\right)}{\sqrt{2}\ln\sigma_i}\right)^2\right],$$

where $D_{m,i}$ and σ_i are the median diameter and geometric standard deviation of the ith mode.

435 The difficulty with applying equilibrium partitioning theory to size distributions is that particles of different sizes have different Kelvin factors and the semi-volatiles will consequently partition non-uniformly across the particles. Connolly et al. (2014) found that when SVOCs condense on to a lognormal size distribution the affect is a change in diameter and geometric standard deviation which maintains the arithmetic standard deviation. When plotted with $\ln D$ on the x axis and $dN/d\ln D$

440 on the y axis this qualitatively looks like a translation in the positive x direction which preserves the shape of the graph. This is especially apparent as the relative humidity reaches 100%. We subsequently replace the Kelvin factors by effective values calculated using the median diameters of the individual size distributions in order to calculate the shift in the size distribution.

Table 5. Parameter values used in the parcel model simulations

variable	n (pcc)	d_m (nm)
mode 1	200	25
mode 2	50	125

The parcel model is run with the parameters given in Table 5 together with the material properties
445 from Table 3 and the second mode is given an initial period of 1500 seconds of simulation time before the smaller mode is added. The subsequent time evolution of the condensed concentrations are shown by the solid lines in Figure 12 for a relative humidity of 0% and 90%. Bulk equilibrium is reached by about 1000 seconds and the parcel model converges on a value which is in good agreement with the partitioning theory shown by the dashed lines.

450 Figure 13 shows the condensed concentrations from Figure 12 on the two individual modes with the left plots showing the smaller mode and right plots showing the larger. Simulations are run for 20000 and 40000 seconds for $R_H = 0\%$ and $R_H = 90\%$ respectively and although the organic shown by the yellow line has not completely reached equilibrium on the first mode it is assumed to be sufficiently close. The condensed concentrations of organics on the larger mode from the partitioning

455 theory are in good agreement with the equilibrium in the parcel model, however, they over predict the concentration on the smaller mode by a factor of two. Due to the total condensed concentrations being in good agreement, an under estimate on the second mode must be accompanied by an over estimate of equal magnitude on the first mode. This then results in a more significant relative error on the first mode because the condensed concentrations are an order of magnitude smaller.

Geoscientific
Model Development
Discussions

460   The equilibrium calculated using the parcel model is further compared against the partitioning
theory in Figure 14 for a range of relative humidities. The stacked bar charts show the proportions
of organics in each volatility bin which are in the vapour phase and the condensed phases on each
mode. Total condensed concentrations from the partitioning theory are shown by the crosses which
lie almost exactly at the top of the red sections which mark the analogous quantity from the parcel
465   model at equilibrium. As previously discussed, the partitioning theory under predicts the condensed
concentrations on the first mode (dashed yellow line) compared to the parcel model (green bar) and
the converse is true for the larger mode (dashed pink line and dashed black lines). The affect of the
increased relative humidity is to increase the total condensed concentration of organics; all of the
organics in the five lowest volatility bins are in the condensed phase even at $R_H = 0\%$ and so this
470   extra organic must come from the higher volatility bins. This is seen by the larger red and green
regions on the higher volatility bins.

Figure 15 shows the size distributions corresponding to Figure 14. Initial lognormal size distribu-
tions for the partitioning theory and parcel model are shown by the pink dashed line and the pale blue
crosses. The size distribution at equilibrium in the parcel model is shown by the solid navy line. To
475   calculate the equivalent line for the partitioning theory we change the diameter and geometric stan-
dard deviation in the lognormal size distribution so that the arithmetic standard deviation remains
constant and the total change in volume of each mode corresponds to the volume of the condensed
organics. The two models can be see to be comparable with little difference in median diameter. The
relative humidity appears to make little difference to the shape of the size distribution with the two
480   peaks simply shifting further to the right at higher values of R_H. Although the final median diameter
of the smaller particles is well approximated the Kelvin factor is more sensitive to errors in diameter
in this range and this is a possible source of the errors in the condensed concentrations seen on the
smaller mode in Figure 14.

8   Conclusions

485   This paper presents both a model and an efficient and accurate method of solution which is suitable
for investigations in a wide range of research areas that use equilibrium partitioning theory. Of par-
ticular interest to the authors is cloud droplet activation parameterisations and, ultimately, inclusion
in global climate models.

The model itself predicts the equilibrium condensed concentrations of organics onto multiple
490   monodisperse aerosol modes incredibly accurately compared to the equilibrium solution from a
dynamic parcel model. When applied to multiple polydisperse aerosol modes with lognormal size
distributions the results are comparable to the limiting behaviour of the parcel model on the larger
aerosol particles but miscalculates for the smaller particles. A suggested cause of this is the errors in
the diameter and consequently the Kelvin factor for particles in the size range used for the smaller

Geoscientific

Model Development

Discussions

EGU

Open Access

495 particles and further work is required to more accurately calculate the change is median diameter
and standard deviation in the lognormal size distribution of the aerosol after co-condensation.

The proposed method of solution is found to be exceptionally accurate for a wide range of parameters. Assuming the same mole fraction for all of the modes offers a quick method of obtaining a reasonably accurate approximation for all but the smallest van't Hoff factors of the core but performs

500 well at high values of R_H. The perturbation correction term offers significant improvements at lower relative humidity, especially for smaller van't Hoff factors, with negligible increase in computational expense.

9 Code Availability

All Matlab source code used in the generation of the plots in this paper, including a solver for the

505 multiple mode equilibrium partitioning theory equations, is available at dx.doi.org/10.5281/zenodo.34025.

Appendix A

The implicit equations governing the quasi-leading order solution can be manipulated to give an explicit expression for each of the condensed concentrations, $\bar{C}_{ij}$, in terms of the average mole fraction. We present the algebra for such a step here. The coupled equations are given by (28) and

510 are restated here

$$\bar{C}_{ij}^c \;=\; \frac{C_j - \sum\limits_r \bar{C}_{rj}^c + \bar{C}_{ij}^c}{1 + \dfrac{C_j^*/\eta_i}{C_i^o(1+\beta)}}.$$

We can make use of the notation given by (14) to write the summation term as $\bar{C}_j^c$ and rearrange the denominator on the right-hand side to give

$$\bar{C}_{ij}^c \;=\; \left(C_j - \bar{C}_j^c + \bar{C}_{ij}^c\right)\frac{C_i^o(1+\beta)}{C_i^o(1+\beta)+C_j^*/\eta_i}.$$

515 The explicit dependence on $\bar{C}_{ij}^c$ can be factorised onto the left-hand side

$$\left(\frac{C_j^*/\eta_i}{C_i^o(1+\beta)+C_j^*/\eta_i}\right)\bar{C}_{ij}^c \;=\; \frac{C_i^o(1+\beta)\left(C_j - \bar{C}_j^c\right)}{C_i^o(1+\beta)+C_j^*/\eta_i},$$

which further reduces to

$$\bar{C}_{ij}^c \;=\; \frac{C_i^o(1+\beta)\left(C_j - \bar{C}_j^c\right)}{C_j^*/\eta_i}. \tag{A1}$$

By summing over i an equation for C_j^c is obtained

520 $$\bar{C}_j^c \;=\; \left(C_j - \bar{C}_j^c\right)\sum_r \frac{C_r^o(1+\beta)}{C_j^*/\eta_r},$$

which has the solution

$$\bar{C}_j^c = \phi_j C_j,$$

where ϕ_j depends on β and η_i and is given by

$$\phi_j(\beta, \eta_i) \quad = \quad \frac{\displaystyle\sum_r \frac{C_r^o(1+\beta)}{C_j^*/\eta_r}}{1 + \displaystyle\sum_r \frac{C_r^o(1+\beta)}{C_j^*/\eta_r}}, \tag{A2}$$

525   The individual condensed concentrations are then be calculated using (A1) which can now be writen

as

$$\bar{C}_{ij}^c \quad = \quad \frac{C_i^o(1+\beta)(1-\phi_j)C_j}{C_j^*/\eta_i}.$$

Appendix B

The details of the linearisation of the perturbation equations (30) are presented in this appendix and

530   we begin by restating the set of non-linear equations

$$\bar{C}_{ij}^c + \hat{C}_{ij}^c = \frac{C_j - \displaystyle\sum_r \bar{C}_{rj}^c + \bar{C}_{ij}^c - \sum_r \hat{C}_{rj}^c + \hat{C}_{ij}^c}{1 + \dfrac{C_j^* \bar{K}_{ij}/\bar{\eta}_i}{C_i^o + \displaystyle\sum_k \bar{C}_{ik}^c + \sum_k \hat{C}_{ik}^c}}.$$

The denominator on the right-hand side can be rearranged to give

$$\bar{C}_{ij}^c + \hat{C}_{ij}^c \quad = \quad \left(C_j - \sum_r \bar{C}_{rj}^c + \bar{C}_{ij}^c - \sum_r \hat{C}_{rj}^c + \hat{C}_{ij}^c \right) \left(\frac{C_i^o + \displaystyle\sum_k \bar{C}_{ik}^c + \sum_k \hat{C}_{ik}^c}{C_i^o + \displaystyle\sum_k \bar{C}_{ik}^c + \sum_k \hat{C}_{ik}^c + C_j^* \bar{K}_{ij}/\bar{\eta}_i} \right)$$

$$= \quad \left(\frac{C_j - \displaystyle\sum_r \bar{C}_{rj}^c + \bar{C}_{ij}^c - \sum_r \hat{C}_{rj}^c + \hat{C}_{ij}^c}{C_i^o + \displaystyle\sum_k \bar{C}_{ik}^c + C_j^* \bar{K}_{ij}/\bar{\eta}_i} \right) \left(\frac{C_i^o + \displaystyle\sum_k \bar{C}_{ik}^c + \sum_k \hat{C}_{ik}^c}{1 + \dfrac{\displaystyle\sum_k \hat{C}_{ik}^c}{C_i^o + \displaystyle\sum_k \bar{C}_{ik}^c + C_j^* \bar{K}_{ij}/\bar{\eta}_i}} \right)$$

535    $$= \quad \left(\frac{C_j - \displaystyle\sum_r \bar{C}_{rj}^c + \bar{C}_{ij}^c - \sum_r \hat{C}_{rj}^c + \hat{C}_{ij}^c}{C_i^o + \displaystyle\sum_k \bar{C}_{ik}^c + C_j^* \bar{K}_{ij}/\bar{\eta}_i} \right) \left(C_i^o + \sum_k \bar{C}_{ik}^c + \sum_k \hat{C}_{ik}^c \right)$$

$$\times \left(1 + \frac{\displaystyle\sum_k \hat{C}_{ik}^c}{C_i^o + \displaystyle\sum_k \bar{C}_{ik}^c + C_j^* \bar{K}_{ij}/\bar{\eta}_i} \right)^{-1}.$$

We now assume that the perturbations are sufficiently small that

$$\left| \frac{\sum_k \hat{C}_{ik}^c}{C_i^o + \sum_k \bar{C}_{ik}^c + C_j^* \bar{K}_{ij}/\bar{\eta}_i} \right| \ll 1, \tag{B1}$$

so that the third term on the right-hand side can be approximated by its Taylor series expansion of the form

$$\frac{1}{1+x} \approx 1 - x + O(x^2),$$

with x equal to the term (B1),

$$\bar{C}_{ij}^c + \hat{C}_{ij}^c = \left(\frac{C_j - \sum_r \bar{C}_{rj}^c + \bar{C}_{ij}^c - \sum_r \hat{C}_{rj}^c + \hat{C}_{ij}^c}{C_i^o + \sum_k \bar{C}_{ik}^c + C_j^* \bar{K}_{ij}/\bar{\eta}_i} \right) \left(C_i^o + \sum_k \bar{C}_{ik}^c + \sum_k \hat{C}_{ik}^c \right)$$

$$\times \left(1 - \frac{\sum_k \hat{C}_{ik}^c}{C_i^o + \sum_k \bar{C}_{ik}^c + C_j^* \bar{K}_{ij}/\bar{\eta}_i} + O\left(\left[\hat{C}_{ij}^c \right]^2 \right) \right).$$

The right-hand side can be linearised assuming the terms of order $O\left(\left[\hat{C}_{ij}^c \right]^2 \right)$ are negligible.

$$\bar{C}_{ij}^c + \hat{C}_{ij}^c = \frac{C_j - \sum_r \bar{C}_{rj}^c + \bar{C}_{ij}^c}{1 + \dfrac{C_j^* \bar{K}_{ij}/\bar{\eta}_i}{C_i^o + \sum_k \bar{C}_{ik}^c}} + \frac{-\sum_r \hat{C}_{rj}^c + \hat{C}_{ij}^c}{1 + \dfrac{C_j^* \bar{K}_{ij}/\bar{\eta}_i}{C_i^o + \sum_k \bar{C}_{ik}^c}}$$

$$+ \left(\frac{C_j - \sum_r \bar{C}_{rj}^c + \bar{C}_{ij}^c}{C_i^o + \sum_k \bar{C}_{ik}^c + C_j^* \bar{K}_{ij}/\bar{\eta}_i} \right) \sum_k \hat{C}_{ik}^c$$

$$- \frac{\left(C_j - \sum_r \bar{C}_{rj}^c + \bar{C}_{ij}^c \right) \left(C_i^o + \sum_k \bar{C}_{ik}^c \right)}{\left(C_i^o + \sum_k \bar{C}_{ik}^c + \dfrac{C_j^* \bar{K}_{ij}}{\bar{\eta}_i} \right)^2} \sum_k \hat{C}_{ik}^c.$$

We can factorise this to give

Geoscientific

Model Development

Discussions

550
$$\hat{C}_{ij}^c + \frac{\sum\limits_r \hat{C}_{rj}^c - \hat{C}_{ij}^c}{1 + \dfrac{C_j^* \bar{K}_{ij}/\bar{\eta}_i}{C_i^o + \sum\limits_k \bar{C}_{ik}^c}} - \left[\frac{\left(C_j - \sum\limits_r \bar{C}_{rj}^c + \bar{C}_{ij}^c\right)\left(C_i^o + \sum\limits_k \bar{C}_{ik}^c\right)\dfrac{C_j^* \bar{K}_{ij}}{\bar{\eta}_i}}{\left(C_i^o + \sum\limits_k \bar{C}_{ik}^c + \dfrac{C_j^* \bar{K}_{ij}}{\bar{\eta}_i}\right)^2} \right] \sum\limits_k \hat{C}_{ik}^c$$

$$= \frac{C_j - \sum\limits_r \bar{C}_{rj}^c + \bar{C}_{ij}^c}{1 + \dfrac{C_j^* \bar{K}_{ij}/\bar{\eta}_i}{C_i^o + \sum\limits_k \bar{C}_{ik}^c}} - \bar{C}_{ij}^c.$$

By denoting the coefficient in the square brackets by $\mathcal{L}_{ij}$ together with

$$\bar{\xi}_{ij} = \left(1 + \frac{C_j^* \bar{K}_{ij}/\bar{\eta}_i}{C_i^o + \sum\limits_k \bar{C}_{ik}^c}\right)^{-1}, \tag{B2}$$

this expresion can be made more notationally simplistic

555 $$\left(1 - \bar{\xi}_{ij}\right)\hat{C}_{ij}^c + \bar{\xi}_{ij} \sum\limits_r \hat{C}_{rk}^c - \mathcal{L}_{ij} \sum\limits_k \hat{C}_{ij}^c = \frac{C_j - \sum\limits_r \bar{C}_{rj}^c + \bar{C}_{ij}^c}{1 + \dfrac{C_j^* \bar{K}_{ij}/\bar{\eta}_i}{C_i^o + \sum\limits_k \bar{C}_{ik}^c}} - \bar{C}_{ij}^c.$$

It is important to note that both $\bar{\xi}_{ij}$ and $\mathcal{L}_{ij}$ depend on the quasi-leading order solution but are independent of the perturbation, $\hat{C}_{ij}$, and as such this equation is now linear in these quantities.

References

Albrecht, B. A.: Aerosols, cloud microphysics and fractional cloudiness, Science, 245, 1227–1230, 1989.

Andreae, M. O. and Crutzen, P. J.: Atmospheric aerosols: biogeochemical sources and role in atmospheric chemistry, Science, 276, 1052–1058, 1997.

Barley, M., Topping, D. O., Jenkin, M. E., and McFiggans, G.: Sensitivities of the absorptive partitioning model of secondary organic aerosol formation to the inclusion of water, Atmospheric Chemistry and Phyics, 9, 2919–2932, 2009.

Biniecka, M. and Caroli, S.: Analytic methods for the quantification of volatile aromatic compounds, Trends in Analytic Chemistry, 30, 2011.

Cai, X. an Griffin, R. J.: Theoretical modeling of the size-dependent influence of surface tension in the absorptive partitioning of semi-volatile organic compounds, Journal of Atmospheric Chemistry, 50, 139–158, 2005.

Cappa, C. D. and Jimenez, J. L.: Quatitative estimates of the volatility of ambient organic aerosol, Atmospheric Chemistry and Phyics, 10, 5409–5424, 2010.

Chýlek, P. and Coakley Jr, J. A.: Aerosols and climate, Science, pp. 75–77, 1974.

Connolly, P., Topping, D. O., Malavelle, F., and McFiggans, G.: A parameterisation for the activation of cloud drops including the effects of semi-volatile organics, Atmospheric Chemistry and Phyics, 14, 2289–2302, 2014.

de Roos, K.: Effect of texture and microstructure on flavour retention and release, International Dairy Journal, 13, 593–605, 2003.

Donahue, N. M., Robinson, A. L., Stanier, C. O., and Pandis, S. N.: Coupled partitioning, dilution and chemical aging of semivolatile organics, Environmental Science and Technology, 40, 2635–2643, 2006.

Dusek, U., Frank, G. P., Hildebrandt, L., Curtius, J., Schneider, J., Walter, S., Chand, D., Drewnick, F., Hings, S., Jung, D., Borrman, S., and Andreae, M. O.: Size matters more than chemistry for cloud-nucleating ability of aerosol particles, Science, 312, 1375–1378, 2006.

Epstein, S. and Gibson, A.: Avoidable Causes of Childhood Cancer, Xlibris, 2013.

Ghan, S. J., Guzman, G., and Abdul-Razzak, H.: Competition Between Sea Salt and Sulphate Particles as Cloud Condensation Nuclei, Journal of the Atmospheric Sciences, 55, 3340–3347, 1998.

Goldstein, A. H. and Galbally, I. E.: Known and unexplored organic constituents in the earth's atmosphere, Environmental Science and Technology, 41, 1514–1521, 2007.

Gray, H. A., Cass, G. R., Huntzicker, J. J., Heyerdahl, E. K., and Rau, J. A.: Characteristics of atmospheric organic and elemental carbon particle concentrations in Los Angeles, Environmental Science and Technology, 20, 580–589, 1986.

Hallquist, M., Wenger, J. C., Baltensperger, U., Rudich, Y., Simpson, D., Claeys, M., Dommen, J., Donahue, N. M., George, C., Goldstein, A. H., Hamilton, J. F., Herrmann, H., Hoffmann, T., Linuma, Y., Jang, M., Jenkin, M. E., Jimenez, J. L., Kiender-Scharr, A., Maenhaut, W., McFiggans, G., Mentel, T. F., Monod, A., Preévôt, A. S. H., Seinfeld, J. H., Surratt, J. D., Szmigielski, R., and Wildt, J.: The formation, properties and impact of secondary organic aerosol: current and emerging issues, Atmospheric Chemistry and Phyics, 9, 5155–5236, 2009.

Hildemann, L. M., Mazurek, M. A., and Cass, G. R.: Quantitative characterization of urban sources of organic
aerosol by high-resolution gas chromatography, Environmental Science and Technology, 25, 1311–1325,
1991.

Hui, Y., Chen, F., Nollet, L., Guine, R., Martin-Belloso, O., Minguez-Mosquera, M., Paliyath, G., Pessoa,
F., Le Quéré, J., Sidhu, J., Sinha, N., and Stanfield, P.: Handbook of Fruit and Vegetable Flavors, Wiley-
Blackwell, 1 edn., 2010.

IPCC: Climate Change 2013: The Physical Science Basis., Cambridge University Press, Cambridge, United
Kingdom and New York, NY, USA, doi:10.1017/CBO9781107415324.004, www.climatechange2013.org,
2013.

Jimenez, J. L. and et. al.: Evolution of organic aerosols in the atmosphere, Science, 326, 1525–1529, 2009.

Klein, R.: Get a Whiff of This, The New Republic, 212, 1995.

Lohmann, U., Feicher, J., Penner, J., and Leaitch, R.: Indirect effect of sulphate and carbonaceous aerosols: a
mechanistic treatment, Journal of Geophysical Research, 105, 12 193–12 206, 2000.

McCormick, R. A. and Ludwig, J. H.: Climate modification by atmospheric aerosols, Science, 156, 1358–1359,
1967.

Mendes, B., Gonçalves, J., and Câmara, J.: Effectivesness of high-throughput miniaturized sorbent- and solid
phase microextraction techniques combined with gas chromatography-mass spectrometry analysis for a rapid
screening of volatile and semi-volatile composition of wines- a comparative study, Talanta, 88, 79–94, 2012.

Morgan, W. T., Allan, J. D., Bower, K. N., Esselborn, M., Harris, B., Henzing, J. S., Highwood, E. J., Kiender-
Scharr, A., McMeeking, G. R., Mensah, A. A., Northway, M. J., Osborne, S., Williams, P. I., Krejci, R., and
Coe, H.: Enhancement of the aerosol direct radiative effect by semi-volatile aerosol components: airborne
measurements in North-Western Europe, Atmospheric Chemistry and Phyics, 10, 8151–8171, 2010.

Morris, E.: Fragrance: the story of perfume from Cleopatra to Chanel, Scriber, 1984.

Odum, J. R., Hoffmann, T., Bowman, F., Collins, D., Flagan, R. C., and Seinfeld, J. H.: Gas/particle partitioning
and secondary organic aerosol yields, Environmental Science and Technology, 30, 2580–2585, 1996.

Pankow, J. F.: An absorptive model of gas/particle partitioning of organic compounds in the atmosphere, Atmo-
spheric Environment, 28, 185–188, 1994.

Pruppacher, H. R. and Klett, J. D.: Microphysics of Clouds and Precipitation, Springer, 2nd edn., 1977.

Rogers, R. and Yau, M. K.: A short course in cloud physics, Butterworth-Heinemann, third edn., 1996.

Sitaramaraju, Y., van Hul, A., Wolfs, K., van Schepdael, A., Hoogmartens, J., and Adams, E.: Static headspace
gas chromatography of (semi-)volatile drugs in pharmaceuticals for topical use, Journal of Pharmaceutical
and Biomedical Analysis, 47, 834–840, 2008.

Stevens, B. and Feingold, G.: Untangling aerosol effects on clouds and precipitation in a buffered system,
Nature, 461, 607–613, 2009.

Topping, D., Connolly, P., and McFiggans, G.: Cloud droplet number enhanced by co-condensation of organic
vapours, Nature Geoscience, 6, 443–446, 2013.

Topping, D. O. and McFiggans, G.: Tight coupling of particle size, number and composition in atmospheric
cloud droplet activation, Atmospheric Chemistry and Phyics, 12, 3253–3260, 2012.

Tsimpidi, A. P., Karydis, V. A., Pozzer, A., Pandis, and Lelieveld, J.: ORACLE (v1.0): modeule to simulate the
organic aerosol composition and evolution in the atmosphere, Geosci. Model Dev., 7, 3153 – 3172, 2014.

Twomey, S.: The nuclei of natural cloud formation part II: the supersaturation in natural clouds and the variation
640   of cloud droplet concentration, Pure and Applied Geophysics, 43, 243–249, 1959.

Twomey, S.: Pollution and the planetary albedo, Atmospheric Science, 8, 1251–1256, 1974.

Twomey, S.: The influence of pollution on the shortwave albedo of clouds, Journal of the Atmospheric Sciences,
34, 1149–1152, 1977.

Vernocchi, P., Ndagijimana, M., Serrazanetti, D., Gianotti, A., Vallicelli, M., and Guerzoni, M.: Influence of
645   starch addition and dough microstructure on fermentation aroma production by yeasts and lactobacilli, Food
Chemistry, 108, 1217–1225, 2008.

Wang, J., MacNeil, J., and Kay, J.: Chemical Analysis of Antibiotic Residues in Food, Wiley, 2011.

Wu, B., Zhang, X., Zhang, X., Yasun, A., Zhang, Y., Zhao, D., Ford, T., and Cheng, S.: Semi-volatile organic
compounds and trace elements in the Yangtze River source of drinking water, Ecotoxicology, 18, 707–714,
650   2009.

Yu, F.: A secondary organics aerosol formulation model considering successive oxidation aging and kinetic con-
densation of organic compounds: global scale implications, Atmospheric Chemistry and Phyics, 11, 1083–
1099, 2011.

Zarra, T., Naddeo, V., Belgiorno, V., and Reiser, M. Kranert, M.: Instrumental characterization of odour: a
655   combination of offactory and analytical methods, Water Science and Technology, 59, 1603–1609, 2009.

Zhang et. al., Q.: Ubiquity and dominance of oxygenated species in organic aerosols in anthropogenically-
influenced Northern Hemisphere midlatitudes, Geophysical Research Letters, 34, 2007.
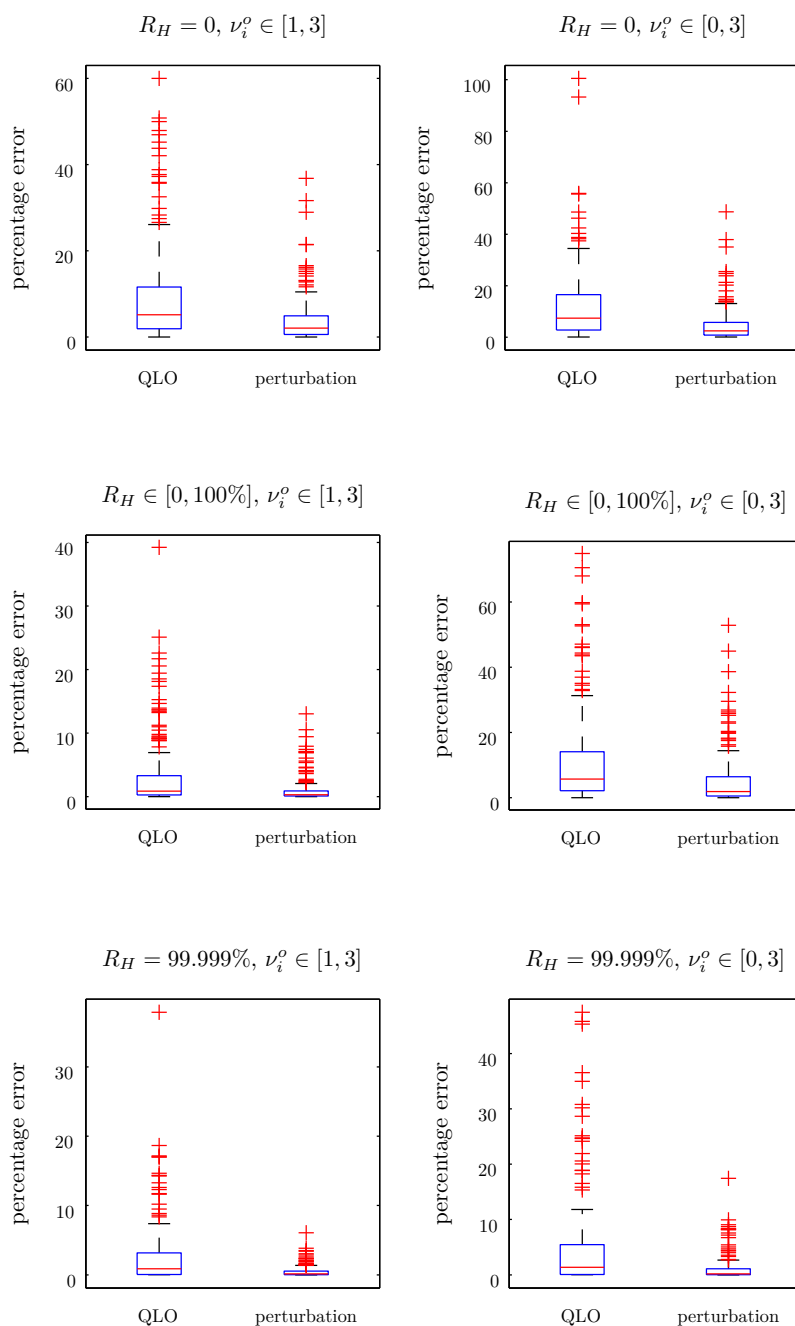
Figure 8. Comparison of the percentage errors in organic mass fraction from the two approximations in relation to those calculated using the non-linear solver for the data points in Figure 7. The quasi-leading order (QLO) and perturbation solutions are shown by the left and right box and whisker plots in each figure, respectively.

Geoscientific
Model Development
Discussions
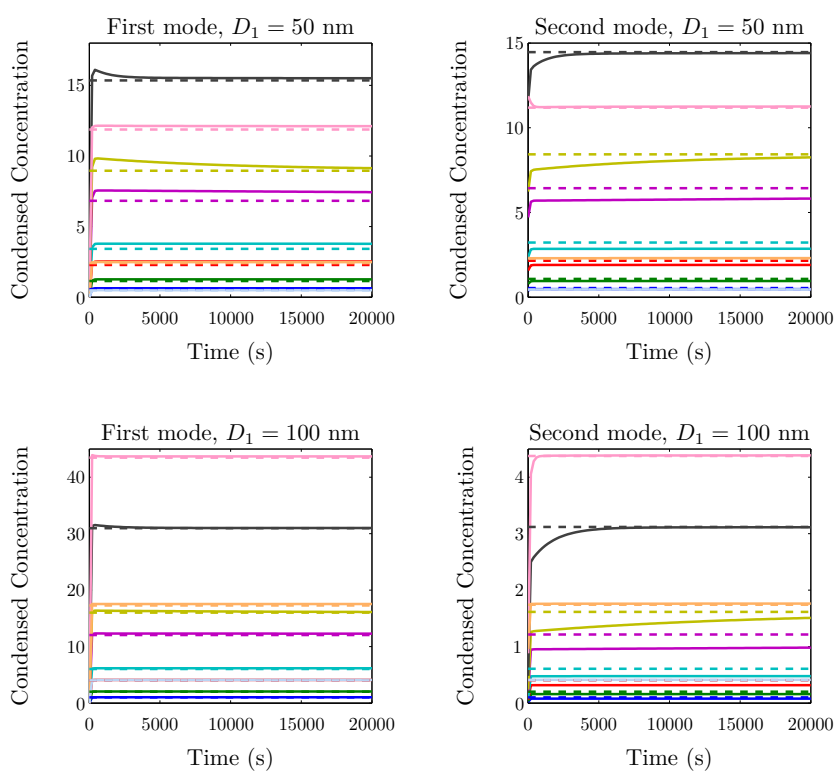
Figure 9. Time evolution of the total condensed concentrations of organics in each volatilty bin in two runs of parcel model (solid lines). The top two plots shown the individual condensed concentrations on each of the modes when the smaller mode has a diameter of 50 nm and the lower two plots show the results when the smaller mode has a diameter of 100 nm. For both runs the number concentration of the first mode was 50 pcc. Each colour represents a different volatility bin and the solution from the partitioning theory is shown by the dashed lines.

Geoscientific
Model Development
Discussions
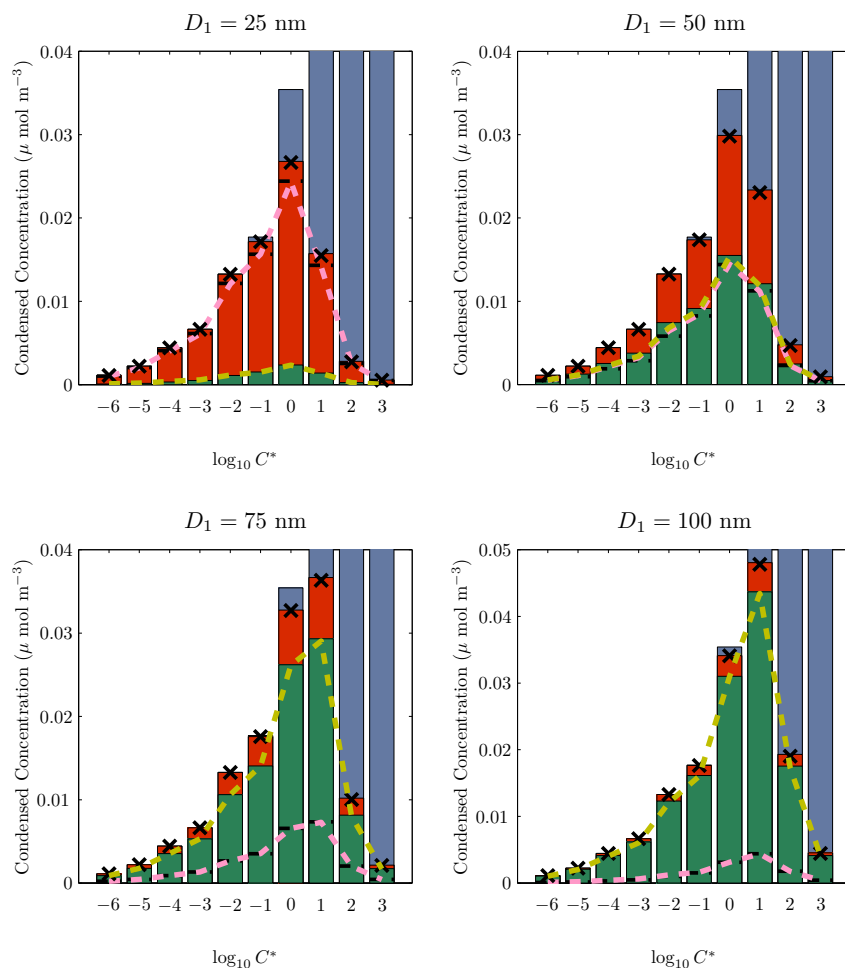
Figure 10. Stacked bar charts showing the condensed concentrations from the two models. Each bar shows the total concentration of organics in each volatility bin and are coloured to show the proportion which is in the vapour phase (blue) and the condensed phases on the first and second modes (green and red respectively). The height of the horizontal black dashed lines across each bar marks the condensed concentrations on the second mode only (the height of the red regions as measured from the x axis). Total concentrations in each volatility bin from the partitioning theory are shown by the black crosses and the amount on the first and second modes are shown by the yellow and pink dashed lines respectively. The y axis is cut off at 0.04 and 0.05 for clarity. The diameter of the first mode is denoted above each plot and the number concentration is 1000 pcc.
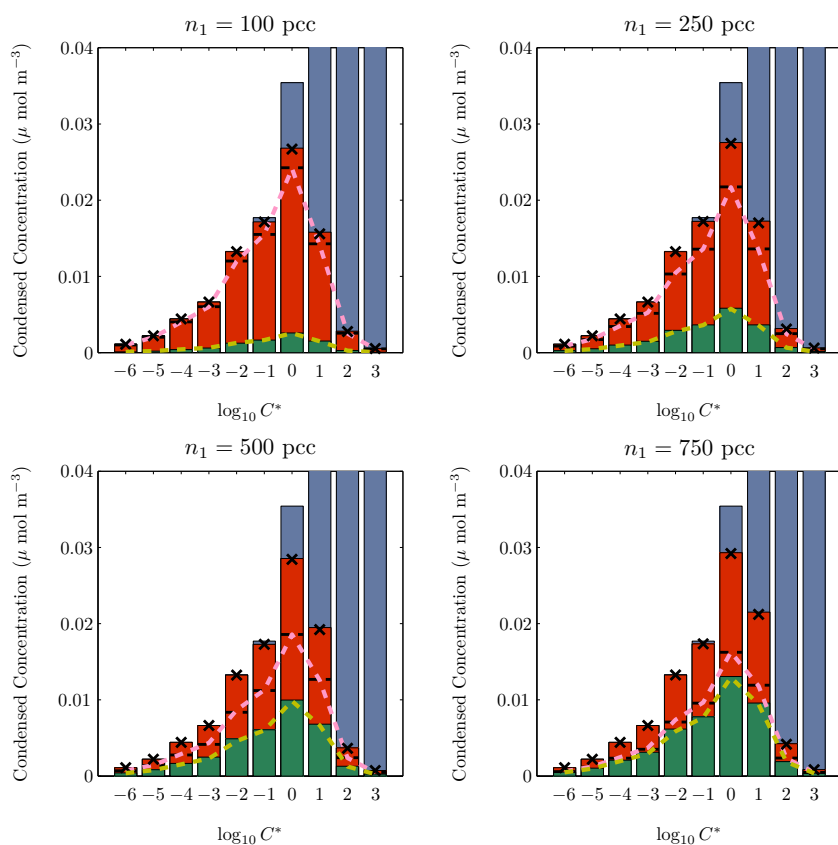
Figure 11. Same as Figure 10 but with differing number concentration in each plot. The diameter of the first mode is 50 nm.
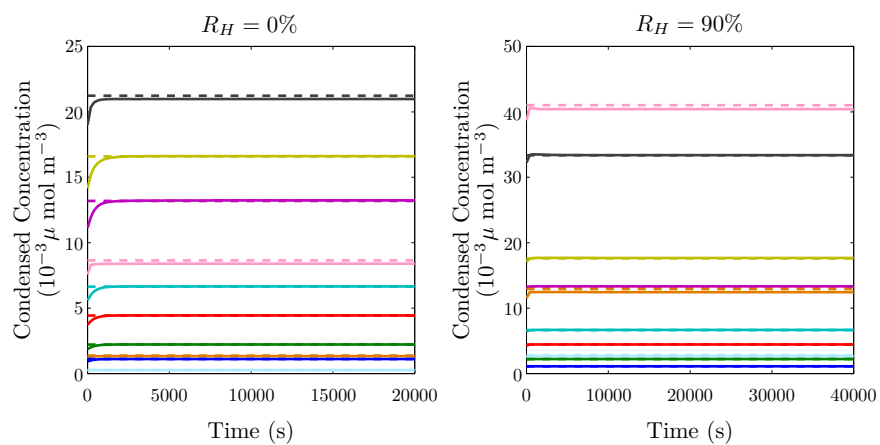
Figure 12. Time evolution of the total condensed concentrations of each organics in the parcel model (solid lines) for $R_H = 0\%$ (left) and $R_H = 90\%$ (right). Each colour represents a different volatility bin and the solution from the partitioning theory is shown by the dashed lines.
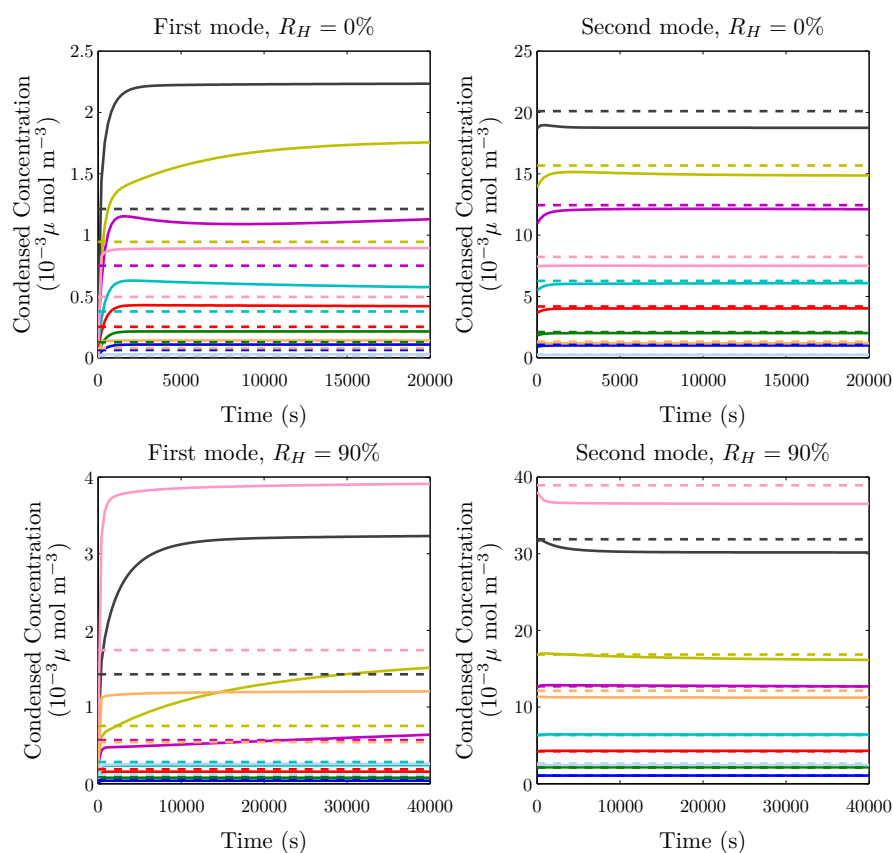
Figure 13. Time evolution of the condensed concentrations on each of the modes in the parcel model (solid lines) for $R_H = 0\%$ (top) and $R_H = 90\%$ (bottom). The smaller mode is shown on the left and the larger on the right. Each colour represents a different volatility bin and the solution from the partitioning theory is shown by the dashed lines.
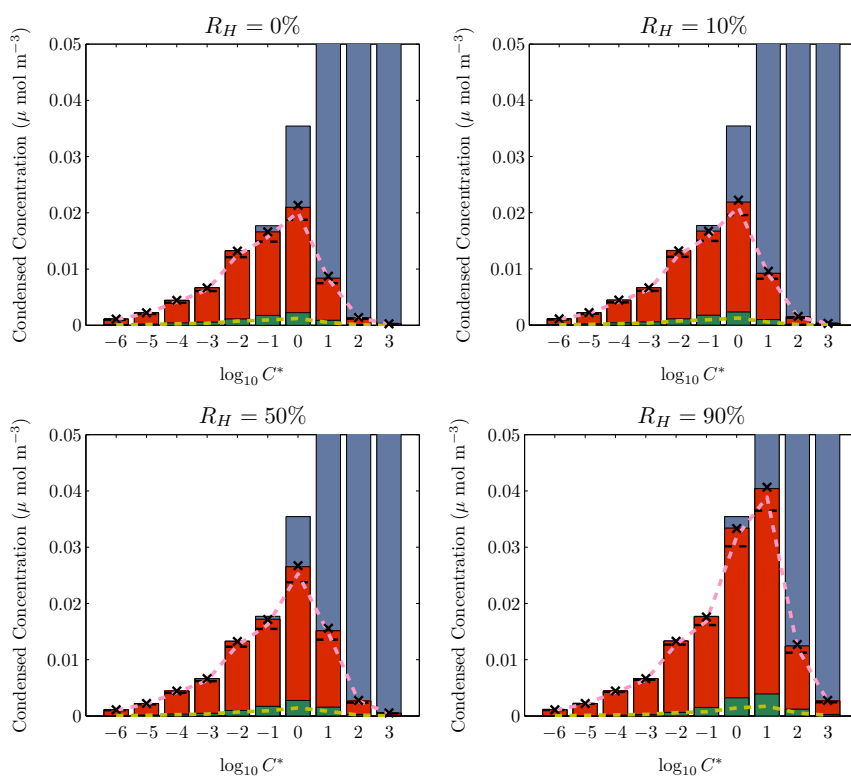
Figure 14. Same as Figure 10 for core aerosol modes represented by lognormal size distributions with number concentrations and median diameters given in Table 5. The relative humidty used in each simulation is stated above each plot.
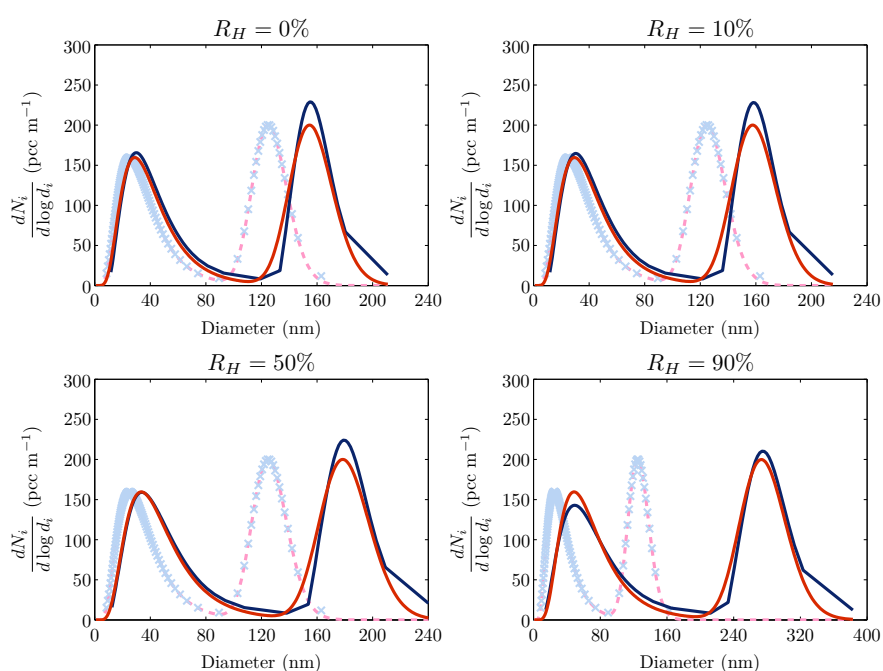
Figure 15. Comparison of the size distribution at equilibrium calculated using the partitioning theory and the parcel model. The initial size distribution at $t = 0$ is shown by the dashed pink line and the pale blue crosses for the partitioning theory and the parcel model respectively. The red lines show the size distribution calculated from the partitioning theory and the navy line shows the equilibrium in the parcel model which is assumed to be at $t = 20,000$ s for $R_H = 0, 10, 50\%$ and $t = 40,000$ s for $R_H = 90\%$.